Cellular dynamical mean-field theory study of an interacting topological honeycomb lattice model at finite temperature

Yao-Hua Chen, Hsiang-Hsuan Hung, Guoxiong Su, Gregory A. Fiete, and C. S. Ting

Cellular dynamical mean-field theory study of an interacting topological honeycomb lattice model at finite temperature

Yao-Hua Chen[1], Hsiang-Hsuan Hung[2], Guoxiong Su[1], Gregory A. Fiete[2], and C. S. Ting[1]

[1]*Texas Center for Superconductivity and Department of Physics,*
University of Houston, Houston, Texas 77204, USA   and
[2]*Department of Physics, The University of Texas at Austin, Austin, Texas 78712, USA*

(Dated: December 22, 2014)

We use cellular dynamical mean field theory with the continuous-time quantum Monte Carlo solver to study the Kane-Mele-Hubbard model supplemented with an additional third-neighbor hopping term. For weak interactions, the third-neighbor hopping term drives a topological phase transition between a topological insulator and a trivial insulator, consistent with previous fermion sign-free quantum Monte Carlo results [H.-Hung *et al.* Phys. Rev. B **89**, 235104 (2014)]. At finite temperatures, the Dirac cones of the zero temperature topological phase boundary give rise to a metallic regime of finite width in the third-neighbor hopping. Furthermore, we extend the range of interactions into the strong coupling regime and find an easy-plane anti-ferromagnetic insulating state across a wide range of third-neighbor hopping at zero temperature. In contrast to the weak coupling regime, no topological phase transition occurs at strong coupling, and the ground state is a trivial anti-ferromagnetic insulating state. A comprehensive finite temperature phase diagram in the interaction-third-neighbor hopping plane is provided.

PACS numbers: 71.30.+h, 75.10.-b, 05.30.Rt, 71.10.Fd

I. INTRODUCTION

Topological insulating states, such as the topological band insulator (TBI), the topological Mott insulator, and other interacting varieties of topological states have attracted much interest in condensed matter physics[1–14]. These topological insulating states are characterized by topological numbers, such as the Chern number, mirror Chern number, and the Z_2 number[15–25]. The TBI have been experimentally found in many materials, such as Bi_2Se_3, and $HgTe/CdTe$ quantum wells[26–33]. Besides the experimental progress in the detection of topological insulating states, much theoretical research has been devoted to the role of lattice geometry on the topological insulating states, including the honeycomb, square, kagome, and more unusual lattices[34–40]. In addition to geometric factors, topological phase transitions can also be induced by a staggered on-site energy[1], Rashba spin-orbit coupling[1–3,26,41], and a third-neighbor hopping in non-interacting models[42,43].

Recently, the influence of electronic correlations on topological states has been the focus of many studies. In the strong coupling limit, interactions could induce magnetic ordering which either breaks the time reversal symmetry, which then spoils the TBI state[35,44–53], or coexists with the topological phases to form an anti-ferromagnetic topological insulator[54–57]. It is also interesting to investigate the topological phase transitions[42,43,58–60] at strong interactions and how finite temperatures influence topological states[61,62]. In particular, interactions and thermal fluctuations have been proposed to drive a nontrivial TBI or otherwise change topological properties[22,38,51,62,63]. Thus, it is highly desirable to investigate the effect of interactions on topological systems, particularly at finite temperature, which is important and relevant to real materials. Recent work has shown that a finite-temperature topological invariant can be defined[64,65], which effectively extends the notation of topological phases to finite temperatures.

Many analytical and numerical methods have been developed to investigate interacting systems in the past few years[66–68], among them dynamical mean-field theory (DMFT) is an especially powerful method capable of capturing the Mott transition[69]. While single-site DMFT has been shown to work well in three dimensional systems (it is exact in the limit of infinite spatial dimensions), in two-dimensional systems non-local correlations and spatial fluctuations can have an important influence on the physics. To improve the predictions of DMFT, particularly in two-dimensions, cellular dynamical mean-field theory (CDMFT)[35,70–74,77,78] has been developed to incorporate spatially extended correlations. In CDMFT, the original lattice is mapped to an effective cluster impurity model coupled to an effective medium. An important impurity solver in CDMFT uses the continuous time quantum Monte Carlo method (CTQMC)[79,80], which is more accurate than the "traditional" discrete-time QMC method. The momentum-dependent spectral function can be used to detect the different characters of the edge states appearing in the topologically trivial and non-trivial states if a strip geometry is used. In addition, topological phase transitions can also be studied by computing the spin Chern number directly in the model we consider because it conserves the z-component of the spin.[43]

In this work, we investigate topological phase transitions in an interacting honeycomb lattice model (a generalized Kane-Mele-Hubbard model–see below) with a third-neighbor hopping, t_{3n}, using CDMFT with the CTQMC solver. At weak interactions, we find a gapped
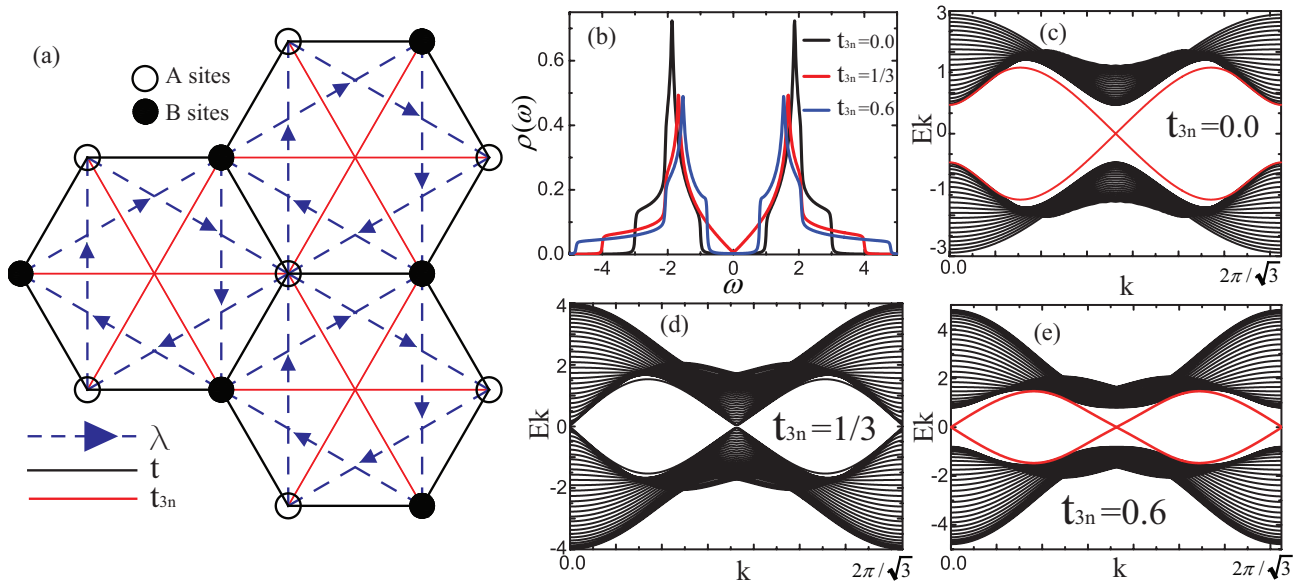
FIG. 1. (Color online) (a) The lattice structure of honeycomb lattice with various hopping parameters described in Eq. (1). (b) The bulk density of states for various values of third-neighbor hopping, t_{3n}, for $\lambda = 0.4, U = 0.0$. (c)-(e) The noninteracting energy bands of Eq. (1) with the zigzag strip geometry for (c) $t_{3n} = 0.0$, (d) $t_{3n} = 1/3$, and (e) $t_{3n} = 0.6$. The width is $N_s = 120$ and spin-orbit coupling is $\lambda = 0.4$. A single Dirac cone is present in (c), indicating a topological state, while two are present in (e), a trivial state. The bulk band gap is closed in (d), as in (b) for $t_{3n} = 1/3$.

topological band insulator with spin Chern number $|C| = 1$ when $t_{3n} = 0$ that persists until $t_{3n} = t_{3n}^c = t/3$, where a gapless metallic state appears. The bulk gap is reopened and spin Chern number $|C| = 2$ when t_{3n} is increased, indicating the system becomes a topologically trivial state (TTI)[43]. Combined with the recent proposal to detect a (spin) Chern number variation in a two-level system via a superconducting qubit[81], it appears that topological phase transitions may be directly observed experimentally. In addition to a change in the topological invariants, topological phase transitions can also be signaled by a gap closing.

In contrast to the zero temperature case[42], we use CDMFT to show the gapless Dirac cone structures at the topological phase boundary give rise to a finite-width (in terms of third-neighbor hopping) metallic state at finite temperatures and finite interactions. This intermediate *metallic* phase exhibits a spin Hall effect, and is one of the main findings of this work. Under strong interactions, an xy-easy plane anti-ferromagnetic insulating state is observed for all values of t_{3n} when the interaction U is beyond a critical value. Thus, there is no topological phase transition in the strong coupling limit. These results are summarized in the finite temperature phase diagram Fig.4, given in the space of interaction strength and the third neighbor hopping. While at finite temperatures our system strictly speaking does not possess long-range order by the Mermin-Wagner theorem, it still possess significant quasi-long range magnetic correlations in the thermodynamic limit at the low-temperatures we study. The interesting phases shown in Fig.4 could be

experimentally probed by transport, angle-resolved photoemission spectroscopy (ARPES)[82], neutron scattering, nuclear magnetic resonance (NMR)[83], and other experimental methods. For interaction values below the critical strength required to induce a magnetic transition, our results are in good quantitative agreement with recent fermion-sign free quantum Monte Carlo calculations on the same model[43]. (The QMC study did not explore the strong coupling regime.)

Our paper is organized as follows. In Sec. II, we introduce the interacting honeycomb lattice model we study, and the cellular dynamical mean field theory. In Sec. III, we present the main results of our CDMFT study, including the spectral function, explicit computations of the edge-state spectrum, and the dependence of various excitation gaps on the parameters of the Hamiltonian. Finally, in Sec. IV we present a finite-temperature phase diagram of our model, which includes an anti-ferromagnetic phase, a topological insulating phase, and a trivial insulating phase. We summarize our results in Sec. V.

II. MODEL AND METHOD

We study the standard Kane-Mele-Hubbard model at half-filling (one electron per site) on the honeycomb lat-

tice:

$$H = -t \sum_{\langle ij \rangle \sigma} c_{i\sigma}^+ c_{j\sigma} + i\lambda \sum_{\langle\langle ij \rangle\rangle} c_{i\sigma}^+ v_{ij}(\sigma) c_{j\sigma}$$
$$-t_{3n} \sum_{\langle\langle\langle ij \rangle\rangle\rangle \sigma} c_{i\sigma}^+ c_{j\sigma} + h.c.$$
$$+U \sum_i n_{i\uparrow} n_{i\downarrow} + \mu \sum_{i\sigma} n_{i\sigma}, \quad (1)$$

where t is the nearest-neighbor (NN) hopping energy, λ is the spin-orbit coupling strength, $v_{ij}(\sigma)$ takes opposite signs for different spin projections and depends on the second-neighbor bond $\langle\langle ij \rangle\rangle$[1,2], t_{3n} is the next-next-nearest-neighbor (NNNN) hopping energy, U is the on-site repulsive interaction, μ is the chemical potential which keeps the system at half filling, $c_{i\sigma}^+$ and $c_{i\sigma}$ denote the creation and annihilation operators respectively, $n_{i\sigma} = c_{i\sigma}^+ c_{i\sigma}$ cis the density operator for spin σ, and σ runs over spin up ($\uparrow$) and spin down ($\downarrow$). Here, we set $t = 1.0$, which is also used as the energy unit in our paper. The spin-orbit coupling strength λ is taken to be $\lambda = 0.4$ throughout. The phase transition that occurs for $U = 0$ as a function of t_{3n} is independent of λ, so long as it has a finite value.

The lattice structure is shown in Fig. 1 (a). The honeycomb lattice can be divided to two sublattices, designated by A sites and B sites. In Fig. 1 (a), the A sites are denoted by white circles, and the black circles shows the B sites. The NN hopping t is shown by the black solid lines, while the blue dash lines describe the spin-orbit coupling strength. The NNNN hopping is demonstrated by the red solid lines. The bulk density of states for various t_{3n} when $\lambda = 0.4$ are shown in Fig. 1 (b). A visible bulk gap opened by the spin-orbit coupling is found when t_{3n} is absent. This bulk gap is closed for $t_{3n} = 1/3$, independent of the value of λ. The gapless behavior means that the system becomes a metal. In contrast to graphene, in the generalized Kane-Mele model, the Dirac cones are located at three time-reversal invariant momenta $M_{1,2} = (\pm\frac{\pi}{\sqrt{3}}, \frac{\pi}{3})$ and $M_3 = (0, \frac{2\pi}{3})$[42,43]. The bulk gap is reopened when $t_{3n} > 1/3$, such as for $t_{3n} = 0.6$. This gapped-gapless-gapped behavior indicates that a topological phase transition may be found when t_{3n} is tuned, and the topological phase boundary is $t_{3n}^c = 1/3$. A direct evaluation of the topological invariant, and band structure computations in a strip geometry confirm this is indeed the case.

Fig. 1 (c)-(d) shows the energy bands in a strip geometry for different t_{3n} when $\lambda = 0.4$, which is obtained with an open boundary condition with zigzag edges. The presence of an odd number of helical edge states (with time-reversed spins) is characteristic of the nontrivial TBI[84]. Clear edge states crossing the bulk gap with one Dirac point are found for $\lambda = 0.4, t_{3n} = 0.0$ in Fig. 1 (c), implying that the system is a topological band insulator, and the spin Chern number $C_\sigma = \pm 1$. Upon increasing t_{3n} to $t_{3n}^c = 1/3$, both the edge and bulk states become gapless (see Fig. 1 (d)), indicating that the system is a

metal (M). When $t_{3n} = 0.6$, the bulk gap reopens and edge states with two Dirac points appear (see Fig. 1 (e)), showing that the state is a topological trivial insulator (TTI). In the trivial case, the spin Chern number $C_\sigma = \pm 2$. As long as S_z is conserved, the spin Chern number is a good quantity to describe the topological properties.

In order to address the Hubbard interaction term in the model given in Eq.(1), we use CDMFT with the CTQMC solver to investigate the topological and magnetic phase transitions on the honeycomb lattice with NNNN (third neighbor, t_{3n}) hopping. In CDMFT, one maps the original lattice model onto an effective cluster model coupled to an effective medium via a standard dynamical mean-field theory (DMFT) procedure.[71] The single-particle Green's function of the cluster, $\hat{g}$, in the effective medium is obtained from

$$[\hat{g}(i\omega)]^{-1} = \frac{1}{\frac{1}{N_k} \sum_{\vec{k}} \frac{1}{i\omega+\mu-\hat{t}(\vec{k})-\hat{\Sigma}(i\omega)}} + \hat{\Sigma}(i\omega), \quad (2)$$

where $\hat{t}(\vec{k})$ is the hopping matrix of the original model Hamiltonian, $\vec{k}$ is the wave vector within the reduced Brillouin zone based on the cluster size and geometry, $\hat{\Sigma}(i\omega)$ is the self-energy, and ω is the Matsubara frequency. The matrix $\hat{g}$ can be used as an input to an impurity solver, such as CTQMC, to obtain the cluster Green's function $\hat{G}_c(i\omega)$ of the physical problem of interest. The new self-energy $\hat{\Sigma}(i\omega)$ is obtained via the Dyson equation $\hat{\Sigma}(i\omega) = \hat{g}^{-1}(i\omega) - \hat{G}_c^{-1}(i\omega)$, and then plugged into Eq. (2) to form a closed self-consistent loop. This loop is iteratively repeated until the self-energy $\hat{\Sigma}(i\omega)$ converges to the desired accuracy. In this paper, we mainly use $N_c = 8$ (N_c is the cluster size) in the bulk CDMFT calculation. The interacting edge spectra are obtained by the momentum-dependent spectral function for the zigzag strip geometry with the width of $N_s = 80$ by using a real-space calculation[75,76]. The details of our choice of the cluster geometry can be found in the appendix of this paper.

The spin Chern number can be obtained by the Green's function at zero frequency and projection operator formalism, the details of which can be found in Ref. [43]. With the Matsubara frequency Green's functions, one can perform an analytical continuation to obtain real frequency Green's functions using the so-called Maximum Entropy Method (MEM)[85]. The density of states $\rho(\omega)$ as well as the single-particle gap ΔE can be obtained from the spectral function $A(\omega) = -\frac{1}{\pi} \text{Im} G(\omega + i\delta)$, where δ is a positive infinitesimal.

At strong interactions, an easy-plane anti-ferromagnetic state develops, and is observed in CDMFT by introducing a symmetry-breaking perturbation in Eq. (1). The Neel temperature T_N decreases as the cluster size N_c increases, eventually tending towards zero[86]. Therefore, in the two-dimensional systems we consider, the Mermin-Wagner theorem is recovered as $N_c \to \infty$. Thus, the anti-ferromagnetic state of Eq. (1) disappears
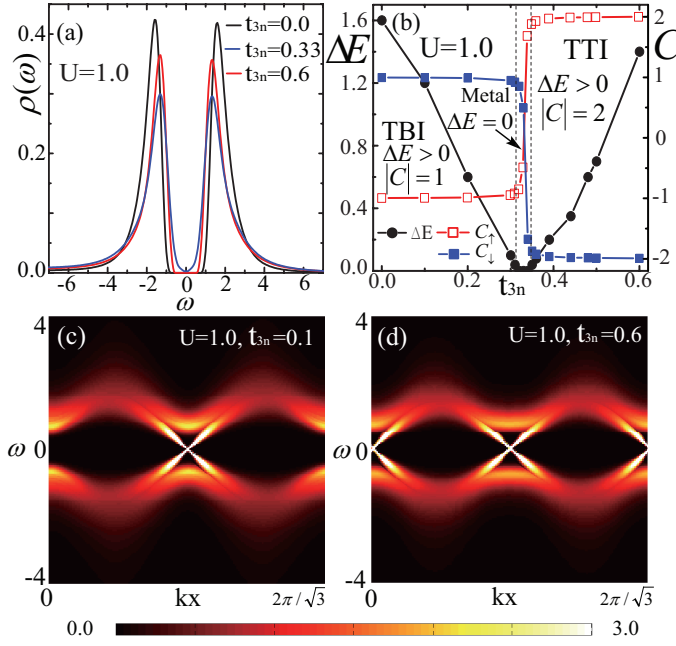
FIG. 2. (Color online) (a) The bulk density of states for different t_{3n} when $\lambda = 0.4, T = 0.05, U = 1.0$. (b)The evolution of the single-particle gap ΔE (left vertical axis) and spin Chern number C_σ (right vertical axis) as a function of t_{3n} when $\lambda = 0.4, T = 0.05, U = 1.0$. (c)-(d) The momentum-dependent spectral function, $A(k,\omega)$, in a strip geometry with $N_s = 80$ for (c) $t_{3n} = 0.0$ and (d) $t_{3n} = 0.6$ when $\lambda = 0.4, T = 0.05, U = 1.0$. By a comparison with Fig. 1, it is clear that (c) is a TBI and (d) is a TTI.

when $N_c \rightarrow \infty$ at finite temperatures. However, for low temperatures, the Mermin-Wagner theorem still allows quasi-long-range order in two dimensional systems with a continuous spin symmetry, as we have here. In an experimental systems of finite size, it may be difficult to distinguish the cases of quasi-long-range order and true long-range order, so we expect our finite cluster results to be meaningful for experiments.

III. RESULTS

A. Hopping parameter-driven topological phase transition

We first focus on the topological phase transition driven by the NNNN hopping, t_{3n}, at weak interactions. Fig. 2 (a) shows the evolution of the density of states (DOS) for different values of t_{3n} when $\lambda = 0.4, U = 1.0, T = 0.05$. Similar to the non-interacting situation, the bulk gap induced by the spin-orbit coupling is present when $t_{3n} = 0.0$. This gap is closed when $t_{3n} = 0.33$, indicating a metallic behavior. Moreover, the gap is re-opened when t_{3n} is increased. This gapped-gapless-gapped behavior indicates that a topological phase tran-

sition can be found when t_{3n} is increased from zero, and this is confirmed by investigating the spin Chern number and the edge modes in a strip geometry. In Fig. 2 (b), we show the development of the single-particle gap ΔE and spin Chern number C_σ as a function of t_{3n} for $\lambda = 0.4, U = 1.0, T = 0.05$, where σ denotes the spin. The single-particle gap ΔE decreases when the t_{3n} is increased towards $1/3$, and the $|C_\sigma| = 1$ character is maintained. When $0.32 < t_{3n} < 0.35$, the ΔE is decreased to zero, indicating the emergence of an intermediate metallic state for finite temperatures. When $t_{3n} > 0.36$, the bulk gap is reopened ($\Delta E \neq 0$) and $|C_\sigma| = 2.0$, indicating that the system becomes a Z_2 TTI. Note that, in the $\Delta E = 0$ regime, the spin Chern numbers Fig. 2 (b) are not quantized, as expected in a metallic state.

The finite parameter extent of the metallic state shown in Fig. 2 (b) is a finite temperature effect. At zero temperature, the sign-free QMC study shows a line-like topological phase boundary[42] when $t_{3n} = t_{3n}^c$. This is because at half-filling the Fermi surface is point-like at t_{3n}^c, with the Dirac points at $M_{1,2,3}$. However, at finite temperatures, thermal fluctuations smear the distribution of electronic states away the Dirac points. Thus, the metallic state can be extended to a finite range of t_{3n}. This behavior has also been observed in graphene[35]. The thermal-fluctuation-induced metallic state exhibits a spin Hall effect. We find that the time-reversal symmetry is still present in this regime, and the presence of spin-orbit coupling in Eq. (1) will bring a spin accumulation on the edges[87,88]. Recent theoretical work also shows that there is a precise sense in which finite temperature topological phases retain a quantized invariant.[64,65] With the caveats mentioned earlier regarding the magnetic order in the strong coupling regime, one may discuss a finite temperature phase diagram for our model that includes both topological phases and magnetic phases.

From Fig. 2, is is clear that even with finite interactions and finite temperature, the helical edges states remain characteristic of the nontrivial topology. In order to check whether the system is truly a topological insulating state for $t_{3n} < 0.31$ and $t_{3n} > 0.36$, we obtain the momentum-dependent spectral function for a strip geometry with an zigzag boundary condition ($N_s = 80$) in Fig. 2 (c) and (d). Clear edge states with one Dirac point are found in Fig. 2 (c), indicating $|C_\sigma| = 1.0$ when $t_{3n} = 0.1$ for $\lambda = 0.4, U = 1.0, T = 0.05$. In Fig. 2 (d), we find edge states with two Dirac points, meaning that $|C_\sigma| = 2.0$. These results are consistent with the evolution of $|C_\sigma|$ as a function of t_{3n}, as shown in Fig. 2 (b).

B. Interaction-driven topological phase transition

Next, we turn to study the topological phase transitions driven by the Hubbard interaction U. In order to study a possible magnetic phase transition in the system, we measure the staggered diagonal magnetic mo-
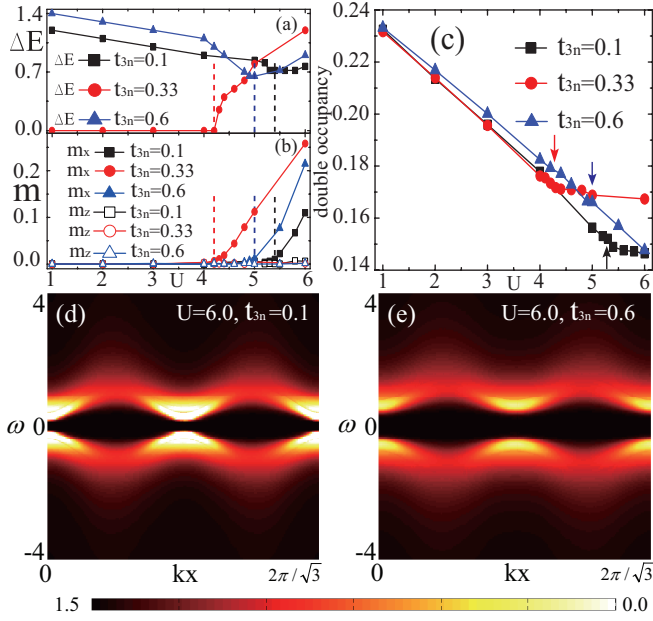
FIG. 3. (Color online) The evolution of (a) bulk single par-
ticle gap ΔE, (b) staggered magnetic moment m_z and trans-
verse magnetism m_x as a function of interaction U when
$\lambda = 0.4, T = 0.05$ for different t_{3n}. The dashed lines show
the critical interaction U_c, which depends on t_{3n}. (c) The
evolution of double occupancy as a function of U, the arrows
show the critical points for different t_{3n} when $\lambda = 0.4, T =
0.05$. (d) - (e): The momentum-dependent spectral function,
$A(k, \omega)$, obtained from the zigzag boundary condition for (d)
$t_{3n} = 0.1$, (e) $t_{3n} = 0.6$ when $\lambda = 0.4, U = 6.0, T = 0.05$.
Note that $U = 6.0 > U_c$ and the spectrum is fully gapped.

ment m_z and the staggered transverse magnetic mo-
ment m_x. The diagonal magnetic moment is defined
as $m_z \equiv \frac{1}{N} \sum_i^N sgn(i)(n_{i\uparrow} - n_{i\downarrow})$, where N denotes the
number of sites in the lattice, i labels the site index
shown in Fig. 1 (a), $sgn(i) = +1$ for i corresponding
to A sites, and $sgn(i) = -1$ for i corresponding to B
sites. The transverse magnetism m_x is defined as $m_x \equiv
\frac{1}{N} \sum_{i=1}^N sgn(i)\langle S_i^x \rangle = \frac{1}{N} \sum_{i=1}^N \frac{1}{2} sgn(i)\langle c_{i\uparrow}^+ c_{i\downarrow} + h.c. \rangle$.

In Fig. 3 (a), we show the evolution of the bulk single-
particle gap ΔE as a function of interaction U for various
t_{3n}. We find that for $\lambda = 0.4, t_{3n} = 0.1, 0.6$, ΔE de-
creases when the interaction U is increased. This means
that the bulk gap induced by the spin-orbital coupling
is suppressed by the interaction. Note, however, that
the single-particle gap *does not close* across the criti-
cal value of interactions where the system become mag-
netic. This is consistent with QMC results obtained on
the Kane-Mele-Hubbard model[44,45]. Different from the
cases of $t_{3n} = 0.1, 0.6$, a gapless behavior is found when
$U < U_c = 4.3$ for $t_{3n} = 0.33$, implying that the system
is a metal over a range of interaction strengths. When
$U > 4.3$ for $t_{3n} = 0.33$, a bulk gap is opened by the
interaction and the system becomes an insulator.

The development of m_z and m_x at various values of

U is shown in Fig. 3 (b), in which the dashed lines show
the critical points U_c for different t_{3n}. When $U > U_c$,
the m_x is increased to a finite value while the m_z re-
mains zero. This indicates a phase transition from a
paramagnetic state to an anti-ferromagnetic insulating
state, which was also found in Kane-Mele-Hubbard model
studies[35,44,45,47]. The finite m_x means that this magnetic
order is formed in the easy-plane. Fig. 3 (c) shows the
evolution of double occupancy d_{occ}, which is defined as
$d_{occ} = \frac{\partial F}{\partial U} = \frac{1}{N} \sum_{i=1}^N \langle n_{i\uparrow} n_{i\downarrow} \rangle$, where F denotes the
energy. The d_{occ} can be used to check the phase tran-
sition order because it is directly connected to the free
energy. In Fig. 3 (c), we find that d_{occ} decreases when
the interaction U is increased, indicating that the itin-
erancy of the particles is suppressed by the interaction.
The arrows in Fig 3 (c) shows the critical points for
different t_{3n}. At the same corresponding Us, the mag-
netic moments develop in Fig. 3 (b). The high d_{occ}
in weak interaction indicates that when $U < U_c$ the ob-
served bulk gap is not induced by the interaction. The
smooth decreasing of d_{occ} indicates that this magnetic
phase transition is likely a second order phase transition.

The presence of a spontaneous easy-plane anti-
ferromagnetic order above a critical interaction strength
mixes the spin components. Thus, S_z is no longer con-
served, spin Chern numbers are not quantized, and there
are gapless Goldstone modes in the spin channel. To
further examine the topological properties of the anti-
ferromagnetic insulating states, we study the edge states
of Eq. (1) at strong coupling. Fig. 3 (d) and (e) show
the momentum-dependent spectral function, $A(k, \omega)$, ob-
tained for the strip geometry with an open boundary
condition for zigzag edges, and periodic boundary con-
ditions for states parallel to the edges. In contrast to
the weak interaction situation, no edge state is found for
$t_{3n} = 0.1$ and 0.6 when $U = 6.0, T = 0.05, \lambda = 0.4$.
This means that across all the values of t_{3n}, the topolog-
ical state is destroyed by the strong interaction, and both
the TBI and TTI are driven to the trivial easy-plane anti-
ferromagnetic insulating state. As a consequence, there
is no topological phase transition as a function of t_{3n} in
the strong coupling limit.

IV. PHASE DIAGRAM

Using CDMFT, we investigate the finite temperature
effects in the Kane-Mele-Hubbard model with third-
neighbor hopping t_{3n}. The phase diagram as a func-
tion of t_{3n} and U is summarized in Fig. 4. When
$U < U_c$, a TBI-M-TTI phase transition occurs when
t_{3n} is increased. The TBI phase can be identified by
$\Delta E \neq 0, |C_\sigma| = 1$, and the TTI state can be found by
$\Delta E \neq 0, |C_\sigma| = 2$, as well as by the different edge states
in the TBI and TTI. A metallic state can be found when
$t_{3n}^{C_{TBI-M}} < t_{3n} < t_{3n}^{C_{M-TTI}}$ with $\Delta E = 0$. Due to the
presence of spin-orbit coupling and time-reversal sym-
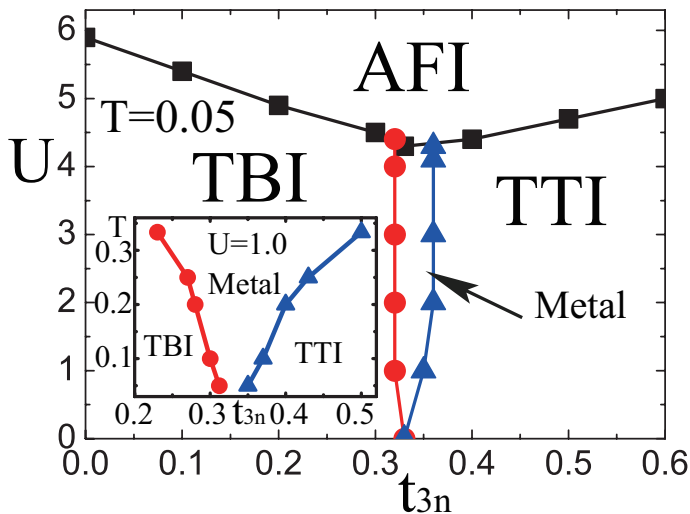metry, at sufficiently low temperature, the metallic state

FIG. 4. (Color online) The $U - t_{3n}$ phase diagram for $T = 0.05$. $\lambda = 0.4$ is considered. TBI: topological band insulator; TTI: topological trivial insulator; AFI: anti-ferromagnetic insulator; M: metal. The inset shows the temperature dependence of the metallic state at $U = 1.0, \lambda = 0.4$.

exhibits a spin Hall effect. The inset of Fig. 4 shows that this metallic state is enlarged when the temperature is increased, but we expect that beyond a certain temperatures (the scale of which would be set by the spin-orbit coupling λ) the spin Hall state effect will vanish. The temperature dependence shown in the inset could be useful for an experiment in which a material is strained (which would change the ratio of t_{3n} to t), and might be used to study the features of the phase diagram we computed.

Fig. 4 shows that an easy-plane anti-ferromagnetic insulating state can be found when the interaction is increased, such as for $U > U_c = 4.3, t_{3n} = 0.33$. A clear gap can be found in the easy-plane anti-ferromagnetic insulating state, in which m_z remains at zero, and m_x is increased to a finite value. The topological property of the magnetic state is further reexamined by studying the edge states using CDMFT and the maximum entropy method. We do not find any coexisting region of a topological state and an anti-ferromagnetic insulating state. We have also considered other cluster sizes and we do not find a strong dependence of the predictions noted above. In the extremed case of $N_c = 2$ (compared to $N_c = 8$ shown in the paper), we find a 10-15% reduction in the single-particle gaps, and a similar shift in the phase boundaries. We therefore conclude that the cluster size does not have an important qualitative effect on our results, aside from the fact that the magnetic transition temperature indeed tends to zero as $N_c \to \infty$, as it should by the Mermin-Wagner theorem.

In earlier QMC work it was noted that for $U < U_c$, the phase boundary between the TBI and TTI phases shifted as a function of interactions in such a way that the TBI phase was "stabilized" by the interactions.[42,43] This feature can also be seen in the CDMFT results shown in Fig. 4: The "center of mass" of the metallic region is shifted to the right compared to the $U = 0$ result. In the earlier QMC work, the origin of the "stabilization" of the topological phase was not understood in detail, though it was remarked that quantum fluctuation effects must be responsible since a straight-forward Hartree-Fock approximation cannot capture the transition.[42,43] However, it was left unclear whether spatial fluctuations or temporal fluctuations are the dominant factor in shifting the phase boundary. Since our CMDFT results contain both short-range spatial fluctuations and temporal fluctuations, we are only able to conclude from our CDMFT results that long-range spatial fluctuations are clearly not the origin of the boundary shift. Fortunately, recent work by some of the authors of this paper have shown that *temporal fluctuations are the most important factor in shifting the phase boundary* to enlarge the topological region of the phase diagram.[89] By *combining* second-order perturbation theory (temporal fluctuations) with a Hartree-Fock approximation (spatially static), the shift of the phase boundary can be quantitatively accounted for.[89]

The combined results of QMC, CDMFT, and perturbation theory followed by Hartree-Fock theory provide a compelling picture for the dominant influence of interactions and finite temperature in the generalized Kane-Mele-Hubbard model we study here. For closely related models with different spatial symmetries[43,89], we believe the CDMFT trends reported here will apply (such as shift of the intermediate, finite-temperature metallic phase *into* the TBI region for models the break the rotational symmetry of the honeycomb lattice).

V. SUMMARY

In summary, we have studied the Kane-Mele-Hubbard model with an additional third neighbor hopping term at finite temperature using cellular dynamical mean-field theory with a continuous-time quantum Monte Carlo impurity solver. The third-neighbor hopping on the honeycomb lattice with spin-orbit coupling can induce a topological phase transition to a trivial state for small interaction values. At finite temperatures, a metallic state with a vanishing single particle gap $\Delta E = 0$ is found in a small region of third-neighbor hopping for interaction values below a certain critical strength. We have computed the temperature dependence of the width of this metallic region, and it is shown in Fig. 4 along with the finite-temperature phase diagram of the model. Recent theoretical work has shown that a quantized topological invariant can be defined for finite temperature systems.[64,65] The metallic region also exhibits a spin Hall effect, as shown in Fig. 2 (b). The finding of this emergent metallic phase at finite temperatures is one of the central results of this paper. Moreover, we have also confirmed

features, such as the shifting of the phase boundary (with interactions), that were earlier reported in QMC but found to be beyond a straight-forward Hartree-Fock approximation.[42,43] This implies that CDMFT may be a reliable tool to study Hamiltonians that have a fermion sign problem in QMC, and thus could be used on a much wider class of Hamiltonians than the one we studied here.

When the interaction is stronger than the critical interaction, an easy-plane anti-ferromagnetic insulating state with transverse magnetic order is formed at zero temperature. For finite temperatures, quasi-long-range order is expected and our finite-size clusters show a magnetic order at finite temperature that vanishes as the number of sites in the cluster tends towards infinity. We find the same magnetic state "above" the topological trivial state and the topological non-trivial state. In addition, we have presented the spectral function of the system for various Hamiltonian parameters through a parameter space representative of the full phase diagram, notably for finite temperatures.

In our study, we did not find any coexisting state of the magnetic order and the Z_2 topological order. Recently, a novel correlated material, Na_2IrO_3, has emerged as a good candidate to investigate the phase transition induced by the interaction and spin-orbit coupling. The relative strength of the NNNN hopping can in principle be adjusted by physical and chemical pressure. It would be interesting to identify experimental systems where our phase diagram could be studied in a real material.

Appendix A: APPENDIX

In the CDMFT[71–74], the original lattice model is mapped onto an effective cluster coupled to environment via a standard DMFT[69] procedure. The Greens function $\hat{g}$ of the effective medium can be obtained by the Dyson equation:

$$\hat{g}^{-1}(i\omega) = \frac{1}{\left(\frac{1}{N_k}\sum_{\vec{k}}\frac{1}{i\omega+\mu-\hat{t}(\vec{k})-\hat{\Sigma}(i\omega)}\right)} + \hat{\Sigma}(i\omega), \quad \text{(A1)}$$

where $\hat{t}(\vec{k})$ is the hopping matrix element in the cluster, $\vec{k}$ the wave vector within the reduced Brioullion
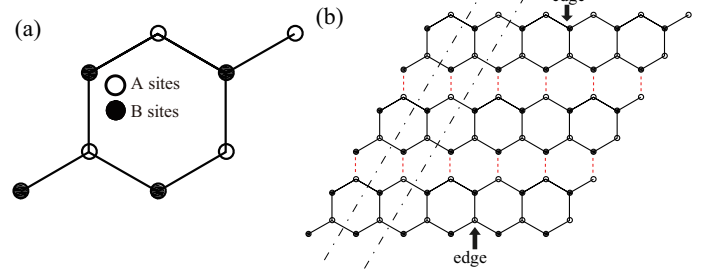

FIG. 5. (Color online) The cluster geometry for (a) bulk CDMFT, (b) realspace CDMFT.

zone based on cluster geometry, ω the Matsubara frequency, and $\hat{\Sigma}(i\omega)$ the self-energy matrix, which must be determine self-consistently. First, one uses an impurity solver, such as the CTQMC[79], to numerically calculate the cluster Green's function $\hat{G}_c(i\omega)$. The updated self-energy $\hat{\Sigma}(i\omega)$ can be calculated by the Dyson equation $\hat{\Sigma}(i\omega) = \hat{g}^{-1}(i\omega) - \hat{G}_c^{-1}(i\omega)$ and is plugged into Eq. (A1). The self-consistent procedure is iteratively repeated until $\hat{\Sigma}(i\omega)$ converges to a desired accuracy (difference after updating is sufficiently small). The size of the self-energy matrix depends on the cluster size and geometry. In the bulk calculations, we used $N_c = 8$, whose geometry is shown in Fig. 5 (a). In this case, the self-energy is a 16×16 matrix (with two spins). The spin Chern number can be obtained by the bulk Green's function at zero frequency $\hat{G}_c(i\omega = 0)$ and projection operator formalism, the details of which can be found in Ref. [43].

On the other hand, the edge spectra are obtained by the momentum-dependent spectral function in a zigzag strip geometry [see Fig. 5 (b)]. In the real-space CDMFT[75,76], the original lattice is mapped to N_s clusters embedded in effective mediums, where N_s is defined as the width of the strip. Due to the presence of the zigzag open edges, the self-energy matrix is a position-dependent function. In our calculations, we chose $N_s = 80$ to have a wide enough strip. The 160×160 self-energy matrix is used in the the self-consistent loop of the real-space CDMFT until self-energy $\hat{\Sigma}(i\omega)$ is converged.

In real space CDMFT, at self-consistency, the momentum-dependent spectral functions are obtained by evaluating the k-dependent Green's function G_k as

$$G_k = \frac{1}{i\omega_n + \mu - eig(\hat{t}_k + \Sigma(\hat{i\omega}))}, \quad \text{(A2)}$$

in which the $\hat{t}_k$ denotes the hopping matrix of the strip used in real space CDMFT, $\hat{\Sigma}(i\omega)$ the self-energy, the $eig(\hat{A})$ the eigenvalue of the matrix $\hat{A}$, ω_n the Matsubara frequency, and μ the chemical potential. Then, we use the Maximum Entropy Method[85] to obtain the spectral function for each eigenvalue of $\tilde{\varepsilon} = \hat{t}_k + \hat{\Sigma}$ for each k.

[1] C. L. Kane, and E. J. Mele, Phys. Rev. Lett **95**, 146802 (2005).

[2] C. L. Kane, and E. J. Mele, Phys. Rev. Lett **95**, 226801 (2005).

[3] D. N. Sheng, Z. Y. Weng, L. Sheng, and F. D. M. Haldane, Phys. Rev. Lett **97**, 036808 (2006).

[4] M. Z. Hasan, and C. L. Kane, Rev. Mod. Phys **82**, 3045 (2010).

[5] X. L. Qi, and S. C. Zhang, Rev. Mod. Phys **83**, 1057 (2010).

[6] C. Z. Chang, J. S. Zhang, X. Feng, J. Shen, Z. C. Zhang, M. H. Guo, K. Li, Y. B. Ou, P. Wei, L. L. Wang, Z. Q. Ji, Y. Feng, S. H. Ji, X. Chen, J. F. Jia, X. Dai, Z. Fang, S. C. Zhang, K. He, Y. Y. Wang, L. Lu, X. C. Ma, Q. K. Xue, Science **340**, 167 (2013).

[7] D. Pesin and L. Balents, Nat. Phys. **6**, 376 (2010).

[8] M. Kargarian, J. Wen, and G. A. Fiete, Phys. Rev. B **83**, 165112 (2011).

[9] J. Maciejko, X. L. Qi, A. Karch, and S. C. Zhang, Phys. Rev. Lett. **105**, 246809 (2010).

[10] X. Wan, A.M. Turner, A. Vishwanath, and S.Y. Savrasov, Phys. Rev. B **83**, 205101 (2011).

[11] A. Go, W. Witczak-Krempa, G.S. Jeon, K. Park, and Y.B. Kim, Phys. Rev. Lett. **109**, 066401 (2012).

[12] A. Ruegg and G.A. Fiete, Phys. Rev. Lett. **108**, 046401 (2012).

[13] J. Maciejko and A. Ruegg, Phys. Rev. B **88**, 241101(R) (2013)

[14] J. Maciejko, V. Chua, and G.A. Fiete, Phys. Rev. Lett. **112**, 016404 (2014).

[15] T. H. Hsieh, H. Lin, J. Liu, W. Duan, A. Bansil, and L. Fu, Nat. Comm. **3**, 982 (2012).

[16] M. Kargarian and G.A. Fiete, Phys. Rev. Lett **110**, 156403 (2013).

[17] A. Shitade, H. Katsura, J. Kuneš, X. L. Qi, S. C. Zhang, and N. Nagaosa, Phys. Rev. Lett **102**, 256403 (2009).

[18] H. J. Zhang, C. X. Liu, X. L. Qi, X. Dai, Z. Fang, and S. C. Zhang, Nature Physics **5**, 438 (2009).

[19] Z. Liu, E. J. Bergholtz, H. Fan, and A. M. Läuchli, Phys. Rev. Lett **109**, 186805 (2012).

[20] H. Z. Lu, J. R. Shi, and S. Q. Shen, Phys. Rev. Lett **107**, 076801 (2011).

[21] D. Xiao, W. Yao, and Q. Niu, Phys. Rev. Lett. **99**, 236809 (2007).

[22] S. Raghu, X. L. Qi, C. Honerkamp, and S. C. Zhang, Phys. Rev. Lett **100**, 156401 (2008).

[23] R. Yu, W. Zhang, H. J. Zhang, S. C. Zhang, X. Dai, and Z. Fang, Science **329**, 5987 (2010).

[24] K. Nomura, S. Ryu, A. Furusaki, and N. Nagaosa, Phys. Rev. Lett **108**, 026802 (2012).

[25] K. Sun, W. V. Liu, A. Hemmerich, and S. D. Sarma, Nature Physics **8**, 67 (2012).

[26] B. A. Bernevig, T. L. Hughes, and S. C. Zhang, Science **314**, 1757 (2006).

[27] D. Hsieh, D. Qian, L. Wray, Y. Xia, Y. S. Hor, R. J. Cave, and M. Z. Hasan, Nature **452**, 970 (2008).

[28] Y. L. Chen, J. G. Analytis, J. H. Chu, Z. K. Liu, S. K. Mo, X. L. Qi, H. J. Zhang, D. H. Lu, X. Dai, Z. Fnag, S. C. Zhang, I. R. Fisher, Z. Hussain, Z. X. Shen, Science **325**, 178 (2009).

[29] Y. Xia, D. Qian, D. Hsieh, L. Wray, A. Pal, H. Lin, A. Bansil, D. Grauer, Y. S. Hor, R. J. Cava, and M. Z. Hasan, Nature Physics **5**, 398 (2009).

[30] S. Chadov, X. L. Qi, J. Kübler, G. H. Fecher, C. Felser, and S. C. Zhang, Nature Materials **9**, 541 (2010).

[31] K. Kuroda, M. Arita, K. Miyamoto, M. Ye, J. Jiang, A. Kimura, E. E. Krasovskii, E. V. Chulkov, H. Iwasawa, T. Okuda, K. Shimada, Y. Ueda, H. Namatame, and M. Taniguchi, Phys. Rev. Lett **105**, 076802 (2010).

[32] H. J. Zhang, S. Chadov, L. Müchler, B. H. Yan, X. L. Qi, J. Kübler, S. C. Zhang, and C. Felser, Phys. Rev. Lett **106**, 156402 (2011).

[33] Z. H. Pan, E. Vescovo, A. V. Fedorov, D. Gardner, Y. S. Lee, S. Chu, G. D. Gu, and T. Valla, Phys. Rev. Lett. **106**, 257004 (2011).

[34] D. Cocks, P. P. Orth, S. Rachel, M. Buchhold, K. Le Hur, and W. Hofstetter, Phys. Rev. Lett **109**, 205303 (2012).

[35] W. Wu, S. Rachel, W. M. Liu, and K. Le Hur, Phys. Rev. B **85**, 205102 (2012).

[36] G. Go, J. H. Park, and J. H. Han, Phys. Rev. B **87**, 155112 (2013).

[37] M. Kargarian and G. A. Fiete, Phys. Rev. B **82**, 085106 (2010).

[38] J. Wen, A. Ruegg, C. C. J. Wang, and G. A. Fiete, Phys. Rev. B **82**, 075125 (2010).

[39] X. Hu, M. Kargarian, and G. A. Fiete, Phys. Rev. B **84**, 155116 (2011).

[40] G. A. Fiete, V. Chua, M. Kargarian, R. Lundgren, A. Ruegg, J. Wen, and V. Zyuzin, Physica E **44**, 845 (2012).

[41] H. H. Lai, and H. H. Hung, Phys. Rev. B **89**, 165135 (2014).

[42] H. H. Hung, L. Wang, Z. C. Gu, and G. A. Fiete, Phys. Rev. B **87**, 121113(R) (2013).

[43] H. H. Hung, V. Chua, L. Wang, and G. A. Fiete, Phys. Rev. B **89**, 235104 (2014).

[44] M. Hohenadler, T. C. Lang, and F. F. Assaad, Phys. Rev. Lett. **106**, 100403 (2011).

[45] M. Hohenadler, Z. Y. Meng, T. C. Lang, S. Wessel, A. Muramatsu, and F. F. Assaad, Phys. Rev. B **85**, 115132 (2012).

[46] D. Zheng, G. M. Zhang, and C. J. Wu, Phys. Rev. B **84**, 205121 (2011).

[47] S. L. Yu, X. C. Xie, and J. X. Li, Phys. Rev. Lett. **107**, 010401 (2011).

[48] S. Rachel, and K. Le Hur, Phys. Rev. B **82**, 075106 (2010).

[49] Y. Yamaji, and M. Imada, Phys. Rev. B **83**, 205122 (2011).

[50] C. Griset, and C. K. Xu, Phys. Rev. B **85**, 045123 (2012).

[51] M. A. N. Araújo, E. V. Castro, and P. D. Sacramento, Phys. Rev. B **87**, 085109 (2013).

[52] J. Reuther, R. Thomale, and S. Rachel, Phys. Rev. B **86**, 155127 (2012).

[53] M. Laubach, J. Reuther, R. Thomale, and S. Rachel, arXiv: 1312.2934.

[54] R. S. K. Mong, A. M. Essin, and J. E. Moore, Phys. Rev. B **81**, 245209 (2010).

[55] C. Fang, M. J. Gilbert, and B. A. Bernevig, Phys. Rev. B **88**, 085406 (2013).

[56] T. Yoshida, R. Peters, S. Fujimoto, and N. Kawakami, Phys. Rev. B **87**, 085134 (2013).

[57] S. Miyakoshi, and Y. Ohta, Phys. Rev. B **87**, 195133 (2013).

[58] T. C. Lang, A. M. Essin, V. Gurarie, and S. Wessel, Phys.

Rev. B **87**, 205101 (2013).

[59] Z. Y. Meng, H. H. Hung, T. C. Lang, Mod. Phys. Lett B, Vol 28, No. 1, 143001 (2014).

[60] Y. H. Chen, J. Li, and C. S. Ting, Physical Review B **88**, 195130 (2013).

[61] T. Yoshida, S. Fujimoto, and N. Kawakami, Phys. Rev. B **85**, 125113 (2012).

[62] Y. X. Zhu, J. He, C. L. Zang, Y. Liang and S. P. Kou, J. Phys.: Condens. Matter **26**, 175601 (2014).

[63] L. Wang, X. Dai and X. C. Xie, Europhysics Letters **98**, 57001 (2012).

[64] Z. Huang and D. P. Arovas, Phys. Rev. Lett. **113**, 076407 (2014).

[65] O. Viyuela, A. Rivas, and M.A. Martin-Delgado, Phys. Rev. Lett. **113**, 076408 (2014).

[66] C. C. Chang and S. W. Zhang, Phys. Rev. Lett. **104**, 116402 (2010).

[67] W. Yao, and Q. Niu, Phys. Rev. Lett. **101**, 106401 (2008).

[68] J. Li, J. An, and C. S. Ting, Phys. Rev. Lett. **109**, 196402 (2012).

[69] A. Georges, G. Kotliar, W. Krauth, and M. J. Rozengerg, Rev. Mod. Phys. **68**, 13 (1996).

[70] O. Parcollet, G. Biroli, and G. Kotliar, Phys. Rev. Lett. **92**, 226402 (2004).

[71] T. Maier, M. Jarrell, T. Pruschke, M. H. Hettler, Rev. Mod. Phys. **77**, 1027 (2005).

[72] G. Kotliar, S. Y. Savrasov, K. Haule, V. S. Oudovenko, O. Parcollet, and C. A. Marianetti, Rev. Mod. Phys. **78**, 865 (2006).

[73] H. Park, K. Haule, and G. Kotliar, Phys. Rev. Lett. **101**, 186403 (2008).

[74] L. DeLeo, M. Civelli, and G. Kotliar, Phys. Rev. Lett. **101**, 256404 (2008).

[75] R. W. Helmes, T. A. Costi, and A. Rosch, Phys. Rev. Lett. **100**, 056403 (2008).

[76] E. V. Gorelik, I. Titvinidze, W. Hofstetter, M. Snoek, and N. Blümer, Phys. Rev. Lett. **105**, 065301 (2010).

[77] C. J. Bolech, S. S. Kancharla, and G. Kotliar, Phys. Rev. B **67**, 075110 (2003).

[78] Y. H. Chen, H. S. Tao, D. X. Yao, and W. M. Liu, Phys. Rev. Lett. **108**, 246402 (2012).

[79] A. N. Rubtsov, V. V. Savkin, and A. I. Lichtenstein, Phys. Rev. B **72**, 035122 (2005).

[80] E. Gull, A. J. Millis, A. I. Lichtenstein, A. N. Rubtsov, M. Troyer, and P. Werner, Rev. Mod. Phys. **83**, 349 (2011).

[81] M. D. Schroer, M. H. Kolodrubetz, W. F. Kindel, M. Sandberg, J. Gao, M. R. Vissers, D. P. Pappas, Anatoli Polkovnikov, and K. W. Lehnert, Phys. Rev. Lett. **113**, 050402 (2014).

[82] A. Damascelli, Z. Hussain, and Z. X. Shen, Rev. Mod. Phys. **75**, 473 (2003).

[83] L. Limot, P. Mendels, G. Collin, C. Mondelli, B. Ouladdiaf, H. Mutka, N. Blanchard, and M. Mekata, Phys. Rev. B **65**, 144447 (2002).

[84] C. J. Wu, B. A. Bernevig, and S. C. Zhang, Phys. Rev. Lett. **96**, 106401 (2006).

[85] M. Jarrell, and J. E. Gubernatis, Phys. Rep. **269**, 133 (1996).

[86] T. A. Maier, M. Jarrell, T. C. Schulthess, P. R. C. Kent, and J. B. White, Phys. Rev. Lett. **95**, 237001 (2005).

[87] J. E. Hirsch, Phys. Rev. Lett. **83**, 1834 (1999).

[88] M. I. Dyakonov, Phys. Rev. Lett. **99**, 126601 (2007).

[89] H. H. Lai, H. H. Hung, and G. A. Fiete, Phys. Rev. B **90**, 195120 (2014).